Weatherill, G., Kotha, S., Cotton, F. (2020): Re-thinking site amplification in regional seismic risk assessment. - Earthquake Spectra, 36, S1, 274-297.

https://doi.org/10.1177/8755293019899956

Re-thinking site amplification in regional seismic risk assessment

GraemeWeatherill[1], Sreeram Reddy Kotha, M.EERI[1], and Fabrice Cotton[1,2]

Abstract
Probabilistic assessment of seismic hazard and risk over a geographical region presents the modeler with challenges in the characterization of the site amplification that are not present in site-specific assessment. Using site-to-site residuals from a ground motion model fit to observations from the Japanese KiK-net database, correlations between measured local amplifications and mappable proxies such as topographic slope and geology are explored. These are used subsequently to develop empirical models describing amplification as a direct function of slope, conditional upon geological period. These correlations also demonstrate the limitations of inferring 30-m shear-wave velocity from slope and applying them directly into ground motion models. Instead, they illustrate the feasibility of deriving spectral acceleration amplification factors directly from sets of observed records, which are calibrated to parameters that can be mapped uniformly on a regional scale. The result is a geologically calibrated amplification model that can be incorporated into national and regional seismic hazard and risk assessment, ensuring that the corresponding total aleatory variability reflects the predictive capability of the mapped site proxy.

Keywords
Earthquake hazard analysis, ground motion, seismic risk, site effects, regional mapping

Introduction

A quantitative estimation of seismic risk is a critical component in the effective mitigation of the threat that earthquakes pose to a structure or to the broader urban environment. Many tenets of probabilistic seismic risk estimation are common both to site-specific analysis, which may be used in the case of estimating the likelihood of damage or loss for a single structure, and to regional analysis, in which the total losses are considered from many properties across a provincial, national, and even multi-national scale. One of the most fundamental differences, however, is in the characterization of the amplification of ground motion due to the local conditions of the site.

For a single site, detailed investigation of the geotechnical properties of the local soils can be expected, and in many cases profiles of shear-wave velocity can be obtained in order to provide the 30-m averaged shear-wave velocity (V_{S30}), from which predictive models of amplification specific to that site are commonly derived. This may often extend to the determination of depth to engineering bedrock, which can be measured directly from the velocity profiles or inferred from horizontal to vertical spectral ratio of ambient microtremor. There are, however, many applications for which it is necessary to infer locally amplified ground motions across a region. In that case detailed site data are

[1] Helmholtz Centre Potsdam, GFZ German Research Centre for Geosciences, Potsdam, Germany
[2] Institute of Geosciences, University of Potsdam, Potsdam, Germany

Corresponding author:
Graeme Weatherill, Helmholtz Centre Potsdam, GFZ German Research Centre for Geosciences, Telegrafenberg, 14467 Potsdam, Germany.
Email: graeme.weatherill@gfz-potsdam.de

available at neither the spatial extent nor resolution required by the model. This applies not only to long-term regional seismic hazard and risk assessment, but also to rapid assessments of losses following damaging events. Models and maps of site conditions inferred from proxies, such as the well-known topographically inferred V_{S30} model of Wald and Allen (2007), in conjunction with the models of site amplification calibrated upon V_{S30} commonly incorporated into ground motion models (GMMs), provide a practical means of incorporating site amplification into regional risk analysis.

While a growing body of literature is dedicated to the improvement or calibration of V_{S30} models inferred from geomorphological and/or geological proxies (e.g., Kwok et al., 2018; Thompson et al., 2014; Thompson and Wald, 2012; Vilanova et al., 2018), it is easy to lose perspective of the purpose that such models serve in terms of risk analysis, which is to characterize the site amplification itself. V_{S30} serves only as a proxy for this purpose. As databases of observed strong motion records expand in size, we find some networks in which many stations have observed repeated ground motions, such that the local amplification of that station can be estimated directly. The Japanese KiK-net strong motion network is the ideal illustration of this (Okada et al., 2004), boasting more than 600 strong motion stations with detailed site velocity profiles, most having recorded multiple seismic events. This invaluable data set is used not for the purpose of refining models of V_{S30} from mappable geological and geomorphological proxies, but to construct models of amplification directly from such proxies. Building on the work of Kotha et al. (2018), who constructed a database of site-to-site amplification with respect to a GMM (hereafter $\delta S2S_S$, explained in the next section) for each of the KiK-net stations, we explore correlations between this amplification and mappable proxies, specifically focusing on slope and geology. This site-to-site amplification term is a relatively recent feature of ground motion modeling and arises from the growth of ground motion data allowing for repeated seismic observations across many stations in a seismic network.

These correlations are intended to assist in calibrating a predictive model of site amplification that not only serve as a practical means of integrating site response into risk assessment on a national or regional scale, but also to ensure that the uncertainties in this approach are incorporated into seismic hazard and risk analysis in an appropriate manner via the aleatory variability of the GMM. It is emphasized here that in this approach it is not necessarily the optimum predictor of ground motion that is sought, such has been the focus of many explorations in site amplification modeling (e.g., Derras et al., 2017), but an appropriate set of mappable predictors that would be capable of making defensible inferences on the degree and extent of site amplification at a regional scale. While the following work does not aim to provide directly an amplification model for Japan, it is emphasized that the methodologies developed herein are intended to form a practical means of incorporating site response into seismic risk calculations at a regional scale. The resulting ground motion amplification models can be integrated directly into the OpenQuake-engine (Pagani et al., 2014), wherein they can be readily implemented into seismic risk analysis for a region, and contribute to the ongoing curation and improvement of seismic hazard and risk models compiled by the Global Earthquake Model.

Components of within-event ground motion variability and correlations with site properties

Site-to-site residual $\delta S2S_S$

For probabilistic seismic hazard and risk analysis, the ground motion Y at spectral period, T, at a site s due to earthquake e is described by a ground motion prediction equation or, more generally, a GMM. Adopting the terminology proposed by Al Atik et al. (2010),

$$\ln Y(T) = f(X_{es}, \theta|T) + \Delta(T) \quad (1)$$

where X_{es} is the vector of explanatory parameters, θ the vector of model coefficients, and Δ a random variable describing the total variability of ground motion assumed to follow a normal distribution such that $\Delta \sim N(\mathbf{0}, \sigma)$. The total variability, σ, is then decomposed into a between-event residual, δB_e, representing the average shift of a population of ground motions from event e from the zero-mean due primarily to the specific properties of the earthquake's source, and the within-event residual, $\delta W_e s$, which is the misfit between a given observation at station s from the median prediction of the specific earthquake. The two residuals themselves follow normal distributions with zero-means and whose variabilities are described as the between-event (τ) and within-event (ϕ) respectively.

With ground motion recording networks now well-established in certain regions, databases of strong motions are likely to include multiple recordings from given stations. Where a sufficient number of strong motion records are available for a given station, the ground motion at station can be defined by

$$\ln Y_{es}|T = \ln\left(Y_{es}^{ref}|T\right) + \ln Amp_{es}(T, X_s) \tag{2}$$

where $\ln\left(Y_{es}^{ref}|T\right)$ refers to the ground motion on a reference site condition (usually rock, though not always as will be seen in due course) and $\ln Amp_{es}(T, X_s)$ a local amplification factor given a set of explanatory site parameters X_s. Convention in ground motion modeling would assume either a linear or nonlinear model relating the amplification factor to the properties of the site such that

$$\ln Amp_{es}(T, X_s) = \mu_{es}^{Amp}(T, X_s) + \delta S2S_S + \delta Amp_{es} \tag{3}$$

where $\mu_{es}^{Amp}(T, X_s)$ is the mean amplification factor given the site characteristics X_s, $\delta S2S_S$ is the site-to-site residual term that represents the systematic deviation of the observed amplification at site s from that predicted by the amplification model, and δAmp_{es} the remaining variability of the amplification factor from one record to another. In this framework $\delta S2S_S$ is an epistemic term for a given site; one that can be defined with repeated observations of ground motion.

Ground motion model and $\delta S2S_S$ data set

The sheer volume of records within the KiK-net data set, with many sites having the number of repeated observations necessary for robust estimation of $\delta S2S_S$, make this the optimum test case for exploring correlations between $\delta S2S_S$ and other parameters. In their analysis of the spectral properties of $\delta S2S_S$ for the KiK-net data, Kotha et al. (2018) derive a GMM from the KiK-net data using the flatfile of Dawood et al. (2016), and it is their resulting estimates of $\delta S2S_S$ for 641 recorded sites used herein. The approach to determine $\delta S2S_S$ adopted by Kotha et al. (2018) differs from that of preceding authors by virtue of the fact that the GMM itself does not include an explicit site amplification term, instead:

$$\ln Y_{es}(T) = f(M_e, R_{es}|T) + \delta B_e(T) + \delta S2S_S(T) + \delta WS_{e,s}(T) \tag{4}$$

in which $\delta WS_{e,s}$ is the residual of the regression capturing record-to-record variability. The site-to-site residual $\delta S2S_S$ and the record-to-record residual $\delta WS_{e,s}$ are then distributed such that $\delta S2S_S \sim \mathcal{N}(\mathbf{0}, \phi_{S2S})$ and $\delta WS_{e,s} \sim \mathcal{N}(\mathbf{0}, \phi_0)$, where ϕ_{S2S} is the between-site variability and ϕ_0 the event- and site-corrected aleatory variability (more commonly the "single-station" standard devia-

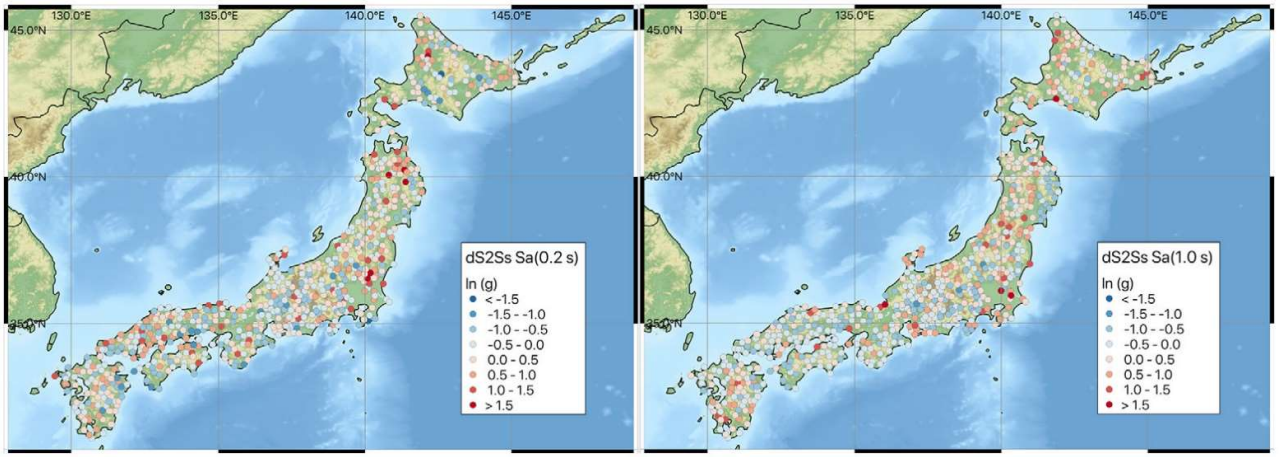

Figure 1. *Observed $\delta S2S_S$ from Kotha et al. (2018) data set.*

tion). In contrast to the estimation of $\delta S2S_S$ outlined in other studies (e.g., Ktenidou et al., 2018; Stewart et al., 2017), in which the term is inferred from existing models from the analysis of repeated ground residuals at a given site, in the current form $\delta S2S_S$ is held as a random effect in the mixed-effects regression of the GMM alongside δB_e. The $\delta S2S_S$ here then describes the local amplification (or de-amplification) of each station with respect to the center of the distribution across all sites.

Figure 1 illustrates how $\delta S2S_S$ varies from station to station across the KiK-net network for 0.2- and 1.0-s spectral acceleration. Not only can differences be seen for between the two spectral periods, clear spatial trends are apparent implying shared amplification properties for nearby station locations. This is of particular importance in the following, as it is this term that will be related to the properties of site in the process of identifying potentially mappable proxies, and subsequently that will be used at the dependent variable for which predictive models of amplification from these proxies can be based.

Limitations of V_{S30} inferred from proxies

Arguably one of the most important practical developments not only for long-term seismic hazard and risk analysis at regional scale but also for real-time loss assessment is the development of the global V_{S3} data set of Wald and Allen (2007). This model is based on the inference of V_{S30} from its correlation with slope, a metric that can be determined from global digital elevation models (DEMs), with alternative calibrations for *active* and *stable* tectonic environments. While the correlation itself is subject to high uncertainty and there exist a range of geological domains in which it can be seen to be especially poor, there exists a reasonable basis upon which it is predicated with respect to the broader geomorphological features influencing site amplification, and as such it provides a practical first-order means of identifying localities where site amplification may be of particular relevance. Attempts to refine or recalibrate estimates of topographically inferred V_{S30} at a local or national scale can be found in the scientific literature (e.g., Lemoine et al., 2012), potentially integrating other geological and/or geomorphological data (e.g., Kwok et al., 2018; Thompson et al., 2014; Thompson and Wald, 2012; Vilanova et al., 2018).

While the application of topographically inferred V_{S30} is particularly useful in a practical sense, where it is routinely misapplied is in its use of an inferred site parameter without increasing the corresponding uncertainty in the GMM. With the exception of a small number of GMMs that explicitly adjust the ground motion aleatory variability for inferred V_{S3} values in order to distinguish them

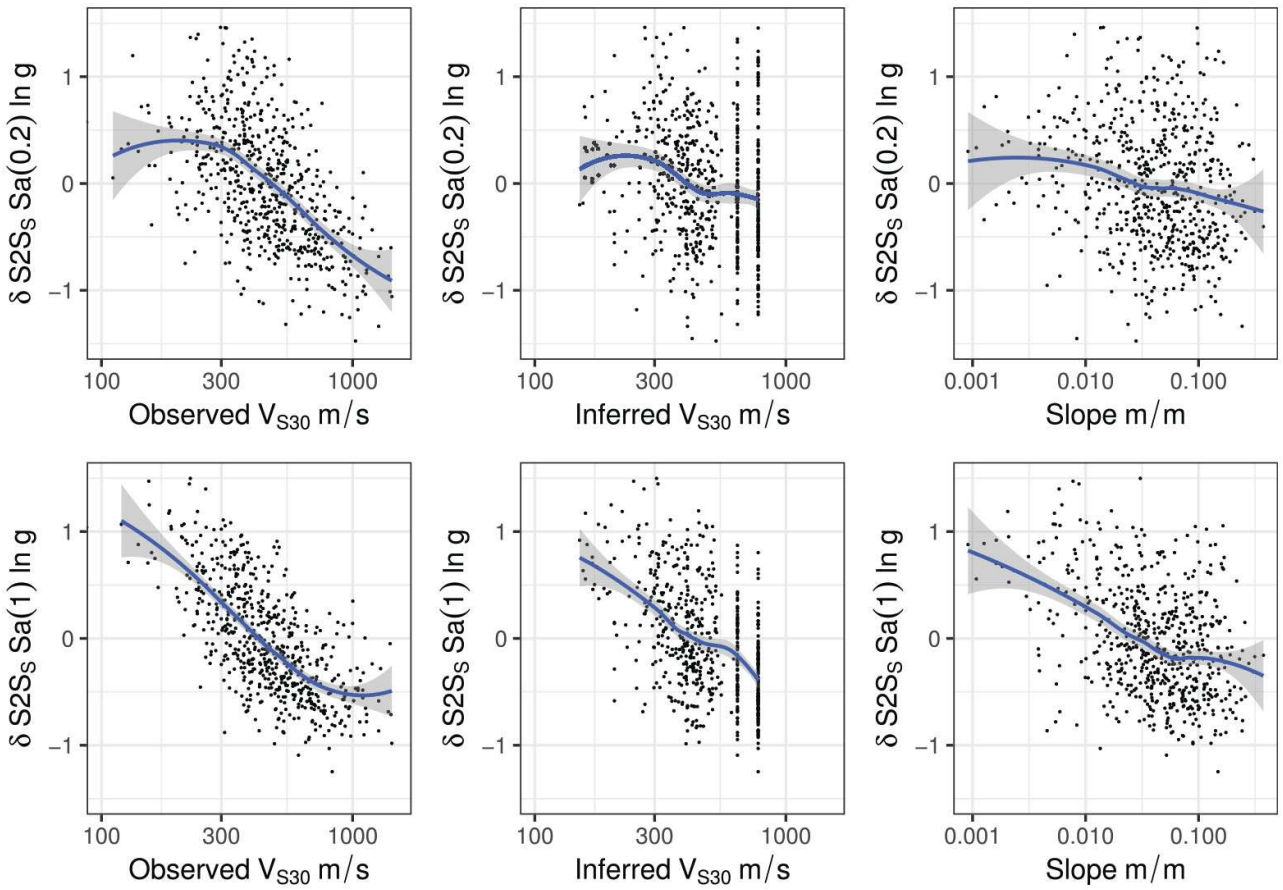

Figure 2. *Correlation between observed $\delta S2S_S$ from Kotha et al. (2018) data set and observed V_{S3} , inferred V_{S30} from Wald and Allen (2007), and slope, fit using a non-parametric LOESS regression (line with shading).*

from the observed V_{S3} case (e.g., Abrahamson et al., 2014; Chiou and Youngs, 2014), the majority of GMMs in the literature make no distinction and often calibrate their amplification models to data that are a mixture of both. As such, an uncertain proxy for V_{S30} is used in conjunction with the GMM's amplification term as if it were a known measured value, which in turn leads ultimately to the uncertainty in the inferred V_{S30} in the site parameter being neglected from the seismic risk calculation entirely.

One can illustrate the impacts of using inferred V_{S30} by considering the KiK-net site data and locally calibrated site-to-site residual of Kotha et al. (2018) that will be described in further detail in the next section. Figure 2 shows that while a relatively strong correlation can be seen between the $\delta S2S_S$ term and the observed V_{S30} for both 0.2 and 1.0-s spectral acceleration, both the correlation with inferred V_{S30} from slope (using the Wald and Allen (2007) approach calibrated for active tectonic regions) and with the slope itself show similar predictive capacities, with weaker correlation and greater uncertainty.

Site data sets mappable at a global scale

Building on previous studies exploring the efficiency of geographical slope in predicting site amplification, one of the most critical data sets is the global DEM. For this purpose, the Shuttle Radar Topography Mission (SRTM30) data set is used, while topographic slope is calculated using the Geospatial Data Abstraction Library (https://gdal.org/). Although higher resolution DEMs are available at a global scale, Allen and Wald (2009) note that although these may resolve small differences in

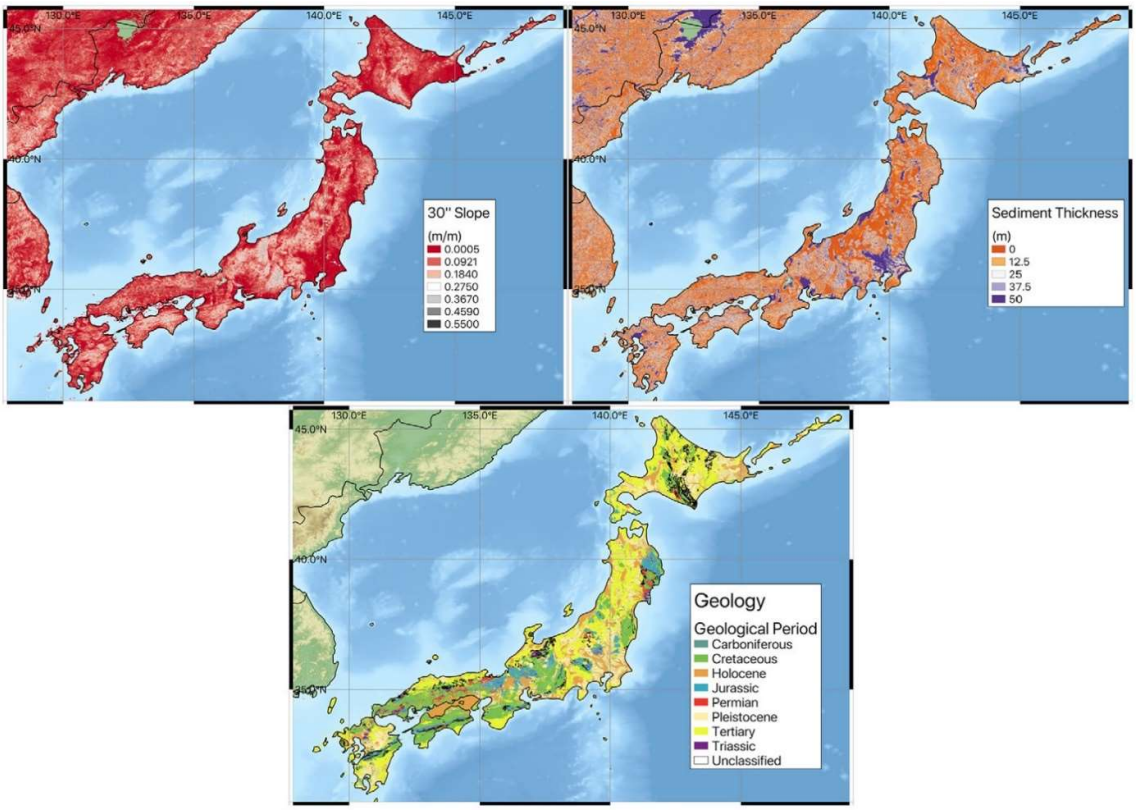

Figure 3. *Mappable site data sets for Japan: slope from SRTM90 (top left), soil and sediment thickness (top right), and geology (bottom).*

gradients for higher slopes they also introduce more variability into the slope calculations, thus reducing the confidence in the correlation with V_{S30}. This observation is contrasted, however, by both Stewart et al. (2017) and Vilanova et al. (2018), who do report a slightly improved correlation at using higher resolution DEMs. To allow adequate comparison with the approach most widely adopted in application; however, for the V_{S3} from topography used herein we maintain the same 30 arc-second DEM resolution adopted by Wald and Allen (2007).

Complementary to the DEM, a global data set of soil, intact regolith, and sedimentary deposit thickness compiled by Pelletier et al. (2016) is also analyzed. This 30-arc-second data set also uses the SRTM digital elevation model as a basis for estimating shallow material thicknesses, based on derived parameters such as curvature and topographic ruggedness index (TRI) to distinguish between upland hillslope and valley bottom, with estimates of shallow sedimentary deposit thickness calibrated accordingly. Although not a direct estimate of basin depth in the sense more commonly encountered in engineering seismology, these data set may provide potential proxies for soil thicknesses that may assist in parameterization of a basin amplification model.

For Japan, a seamless geological map is available at 1:200,000 scale (see Figure 3; Geological Survey of Japan, 2014), which will form a critical data set for categorizing sites. With an immense spatial coverage, the digital data set defines for almost every polygon an estimate of age (according to geological epoch, or range of epochs), a general description and a lithological description.

Exploring correlations

The data set of 641 site observations and the associated parameters inferred from mapped data permit exploration of a variety of potential correlations that may be of interest for characterizing site amplification. A defining factor here is the inclusion of a geological classification from the digital

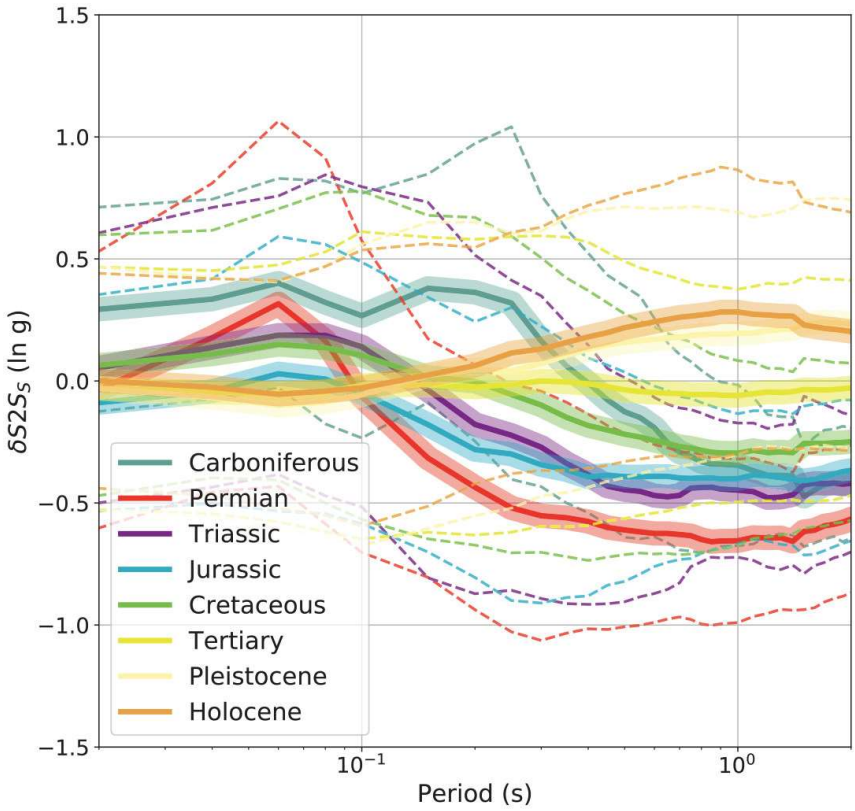

Figure 4. *Number of KiK-net stations in each geological period.*

geological map of Japan. In exploring these correlations, a preliminary subdivision of the data set is made in order to attempt to identify stations in different geological conditions. The initial question, however, is what level of resolution in geological properties could be obtained from the data to permit meaningful analysis to be undertaken. With over 150,000 individual geological units mapped in the digital data set, attempting a unit-by unit analysis would be impossible. Instead, the international standard on chronostratigraphic classification is adopted to assign each unit to a geological period based on the latest epoch described in the range. Given the geological history of Japan, and considering the distribution of KiK-net sites within each geological period, a total of eight periods are found: Carboniferous, Permian, Jurassic, Triassic, Cretaceous, Tertiary (combining both the Paleogene and Neogene periods), Pleistocene and Holocene. The 641 KiK-net sites with measured $\delta S2S_S$ values are then assigned to their respective geological periods.

A critical point to address before exploring more deeply the correlations is the resolution of the geological categorization that should be undertaken for analysis. The geological data set used here provides information on the lithology, the general geological age, and the epoch of each unit. The 641 KiK-net sites considered here are divided between 64 different lithological units and 43 different age categories. Instead, a better balance can be struck between number of stations per geological category when considering only the geological period. The number of records and the distribution of measured V_{S30} values in each period are shown in Figure 4. However, it can also be seen that in the pre-Cretaceous periods (Carboniferous, Permian, Triassic, and Jurassic) fewer than 30 stations are present, with as few as five in the Carboniferous. It will be seen in due course from the exploration of correlations between the site properties and amplifications that significant differences between the four pre-Cretaceous periods are virtually impossible to discern, and would have a minimal impact on resulting geologically dependent models. Subsequently, therefore, we group these four geological

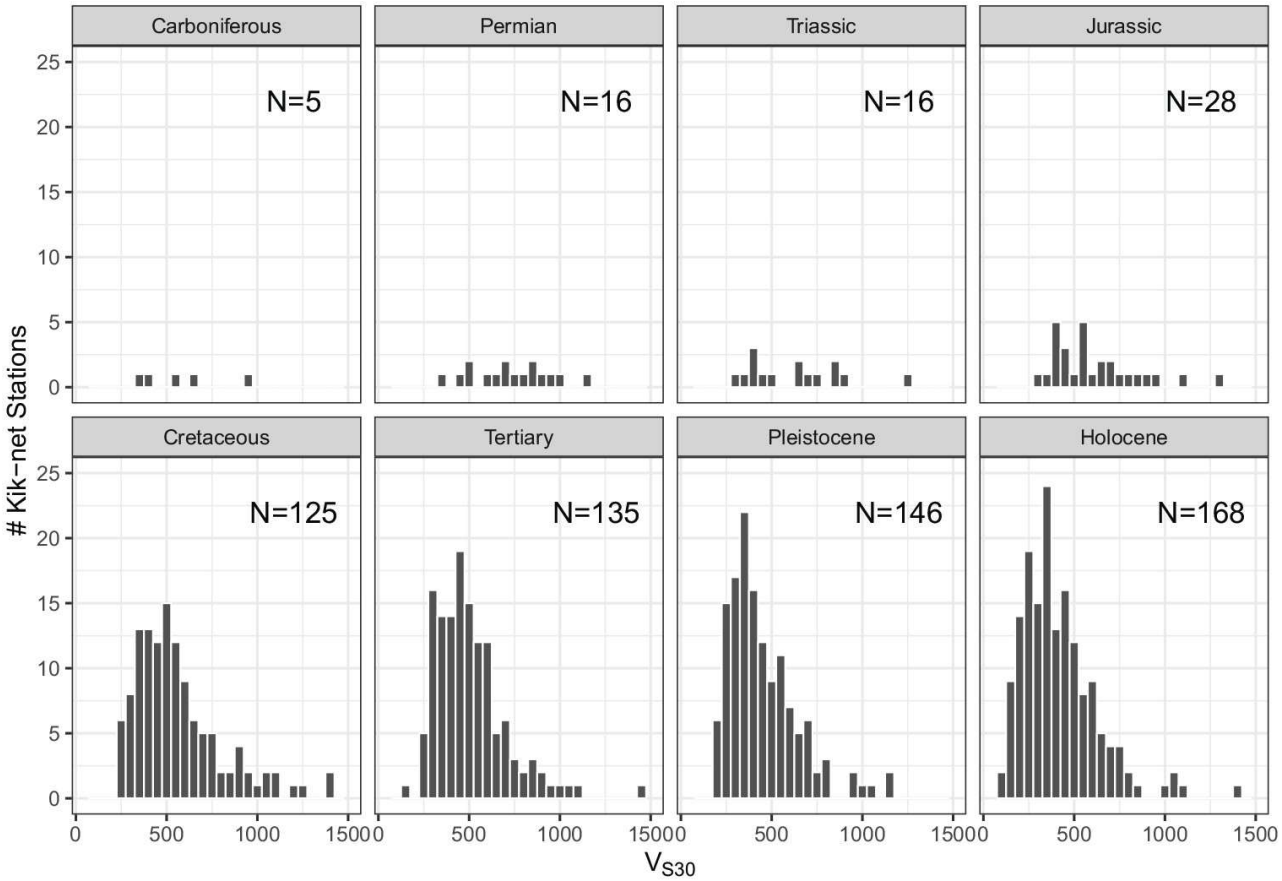

Figure 5. *Variation in $\delta S2S_S$ spectral period, organized by geological era and period.*

periods into a single "Pre-Cretaceous" category.

Using the $\delta S2S_S$ values provided by Kotha et al. (2018), we explore the general distribution of values within each geological class to identify if geological trends are present in the site-to-site residual data. Figure 5 shows both the individual distribution of $\delta S2S_S$ across the 0.02- to 2-s spectra for each of the sites, with the mean trends per geological unit highlighted. Consistent with our expectations, we find that older geological units (Jurassic, Triassic, and Permian) tend toward negative $\delta S2S_S$ at periods greater than 0.1 s, with weakly positive values at very high frequencies. In contrast, Quaternary units (Holocene and Pleistocene) show higher positive $\delta S2S_S$ values at periods greater than 0.1–0.2 s. Tertiary and Cretaceous units tend to fall closer to the $\delta S2S_S = 0$ line, suggesting it is representative of the center of the data set. Five sites were found to be located in Carboniferous domains, most of which within accretionary complexes. As the properties (e.g., V_{S30}, soil thickness) of these five sites are highly variable, very little could be inferred from this small sample as to the general variability within this domain.

Although not the primary target of this work, the assignment of geological conditions to the KiK-net sites also permits one to explore correlations between observed V_{S3} , as measured directly from the velocity profiles provided for each station in the KiK-net data set (Okada et al., 2004), and slope within each geological period, Figure 6. It is quite obvious from this comparison that the relation

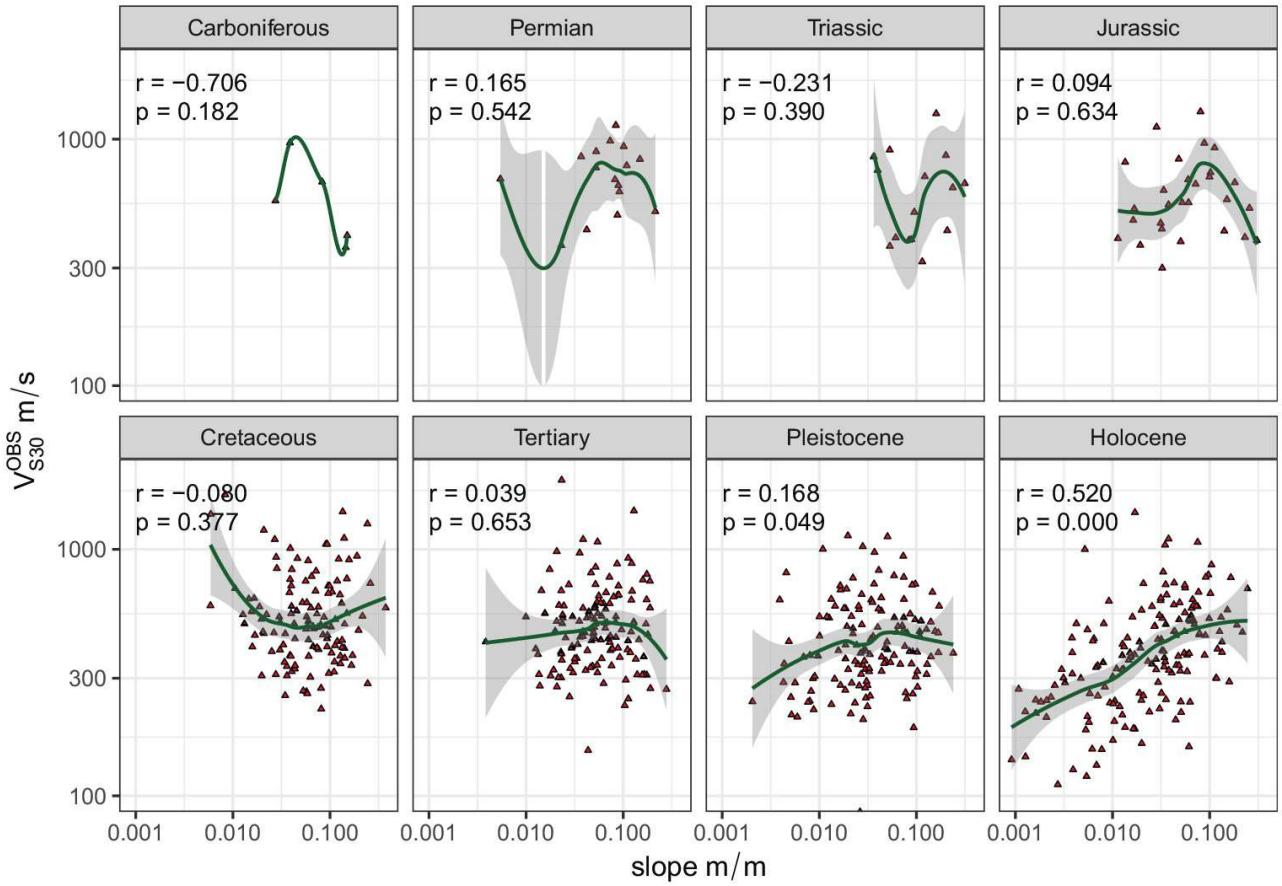

Figure 6. *Correlations between measured V_{S30} and slope organized by geological period, with trends indicated by LOESS smoothing (line with shading). Pearson product-moment values and correlation significance levels indicated by the r and p values respectively.*

between slope and V_{S30} has a dependence on the general geological environment, with correlations of statistical significance achieved only for Quaternary sites (as shown by the p values in Figure 6). Sites in older environments (Cretaceous and earlier) are predominantly located in upland regions of Japan where slopes tend to be somewhat higher and the terrain rougher. In these cases, V_{30} may depend much more on local scale geomorphological features, such as narrow upland valleys or hillside terrain, which may not necessarily be resolved by the slope at this spatial resolution.

Figures 7 and 8 illustrate how these trends between $\delta S2S_S$ and slope can be deconstructed by geological period for different spectral accelerations. The general trends in the data set are illustrated using a non-parametric locally estimated scatterplot smoothing algorithm (LOESS), shown in blue lines on these and subsequent plots. Two obvious trends emerge, both of which are evident in the LOESS regression lines. The first is that the correlation between slope and amplification is mostly constrained to younger geological environments (Tertiary and Quaternary) and that in this current data set there is very little evidence of amplification at all within Cretaceous and Pre-Cretaceous domains. The second trend is that correlations in amplification with slope are more visible in intermediate-to long-period motion than for short-period motion.

The weakness of the slope and amplification correlations in older terrains is indicative of the environments in which older and more consolidated material and rock formations are closer to the surface than in the Pleistocene and Holocene depositional environments. As such, there is a tendency for stations to be found in upland or mountainous areas, with steeper slopes and thinner layers of deposits. It can be seen in both Figures 7 and 8 that for Pre-Cretaceous data set, not only is there no

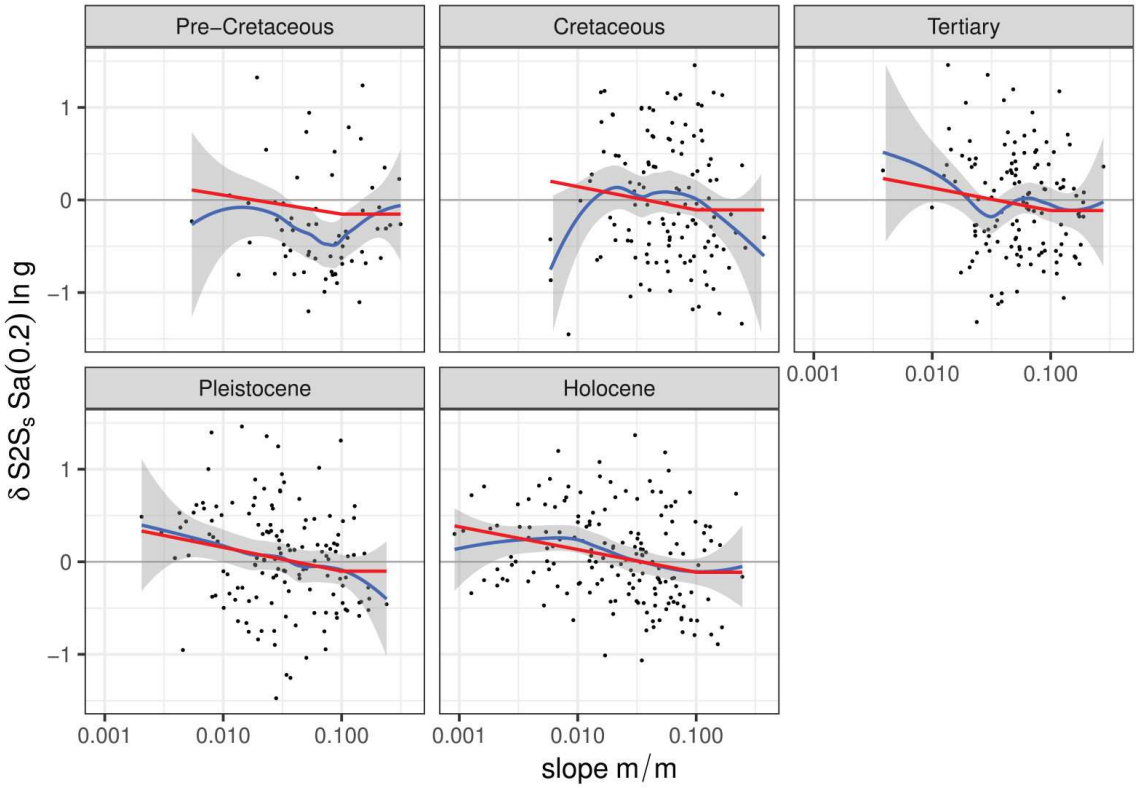

Figure 7. *Trends between $\delta S2S_S$ at Sa(0.2 s) and slope by geological period with non-parametric LOESS regression indicated by blue lines with shading and the predictive model from mixed effects regression (Equation 5) overlain in red.*

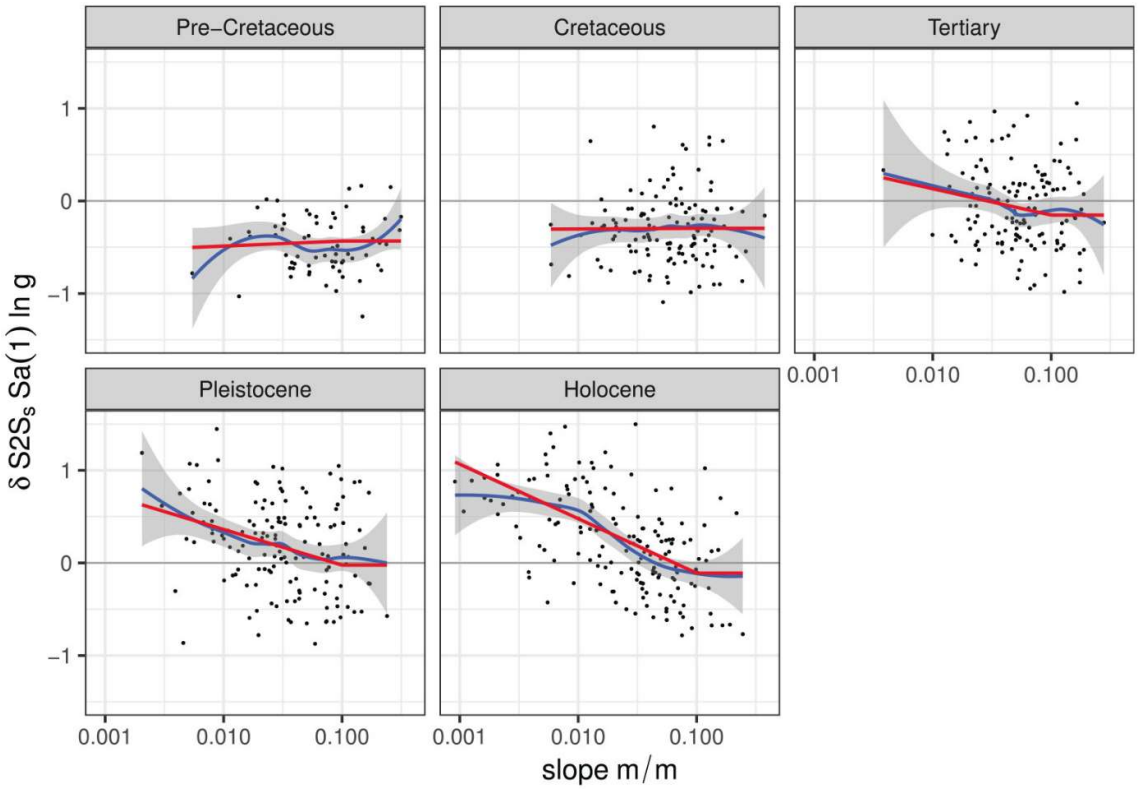

Figure 8. *As Figure 7 for Sa(1.0 s).*

discernable trend with slope, there is also a predominantly negative $\delta S2S_S$ indicating de-amplification with respect to the center of the data set.

The dependence of the correlation between slope and $\delta S2S_S$ upon the spectral period is consistent with trends commonly observed in amplification models, with greater long-period amplification in softer and thicker soils typically associated with younger depositional environments. The weakening of this trend at shorter periods, tending toward a slightly positive amplification for older sites at higher frequencies, could also suggest evidence of influence of k_0 in the amplification, where k_0 is the site-specific component of k (the rapid decay of observed ground motion Fourier spectra at high frequencies with respect to a ω^2 source model). Those few sites classed as Carboniferous are illustrative of this, as most of these sites tend to be located on steeper slopes within accretionary terrains, with higher shear-wave velocities and relatively shallow depths to bedrock.

By grouping those KiK-net sites by geological period we see that there exist key environments for which the relation between slope and site amplification does not hold. Mostly, however, these are environments in which the surficial geology comprises older, harder materials, which one would typically expect to de-amplify motion with respect to the "average" site condition (in this case in the range $500 \leq V_{S30}(m/s) \leq 600$). By contrast the correlation between slope and amplification is arguably at its strongest in the Quaternary environments (Holocene and Pleistocene). From this assessment we find that correlations between slope, geology, and site amplification demonstrate the limitations of inferring V_{S30} from slope and applying these directly into GMMs. As both slope and geology are mappable at a regional scale, however, it is possible to leverage on this information to derive models of amplification that are calibrated to these parameters and thus apply them over a larger spatial domain.

Deriving a site amplification model from $\delta S2S_S$ and geology

The influence of geology in the slope-to- $\delta S2S_S$ correlations shown in Figures 7 and 8 has the potential to be exploited to produce models of site amplification that are applicable on a regional scale. We define a simple parametric function to fit the correlation between slope and $\delta S2S_S$ conditional upon the geological environment. For this purpose, a linear mixed effect model is adopted (Bates et al., 2015), using geological period as a random effect. Recognizing, as previous authors have done, that even in spite of the inherent uncertainty in the relation between slope and V_{S30} the two quantities scale linearly in logarithmic space, we adopt a simple two-segment piecewise linear form for the fixed effect model:

$$\delta S2S_S = \begin{cases} (c_1|\text{geology}) \cdot \ln \dfrac{slope}{(c_2|\text{geology})} + \varepsilon\sigma_s & slope < x_c \\ (c_1|\text{geology}) \cdot \ln \dfrac{x_c}{(c_2|\text{geology})} + \varepsilon\sigma_s & slope \geq x_c \end{cases} \quad (5)$$

where $slope$ is reported in m/m, geology refers to the geological period and is treated as a random effect for within this regression, c_1 and c_2 are fit by the model and x_c a breakpoint in the piecewise scaling, and σ_s is the remaining site-to-site variability. The break in scaling is introduced to fix the $\delta S2S_S$ for steep slopes where data are poorly constrained. This was initially held as a parameter to be optimized by the regressions; however, it was found to be largely insensitive to the spectral period, T, and holding it as a free parameter led to sub-optimal convergence in cases where trends between $slope$ and $\delta S2S_S$ were poorer. In the regression analysis x_c is held fixed at 0.1 m/m. In contrast

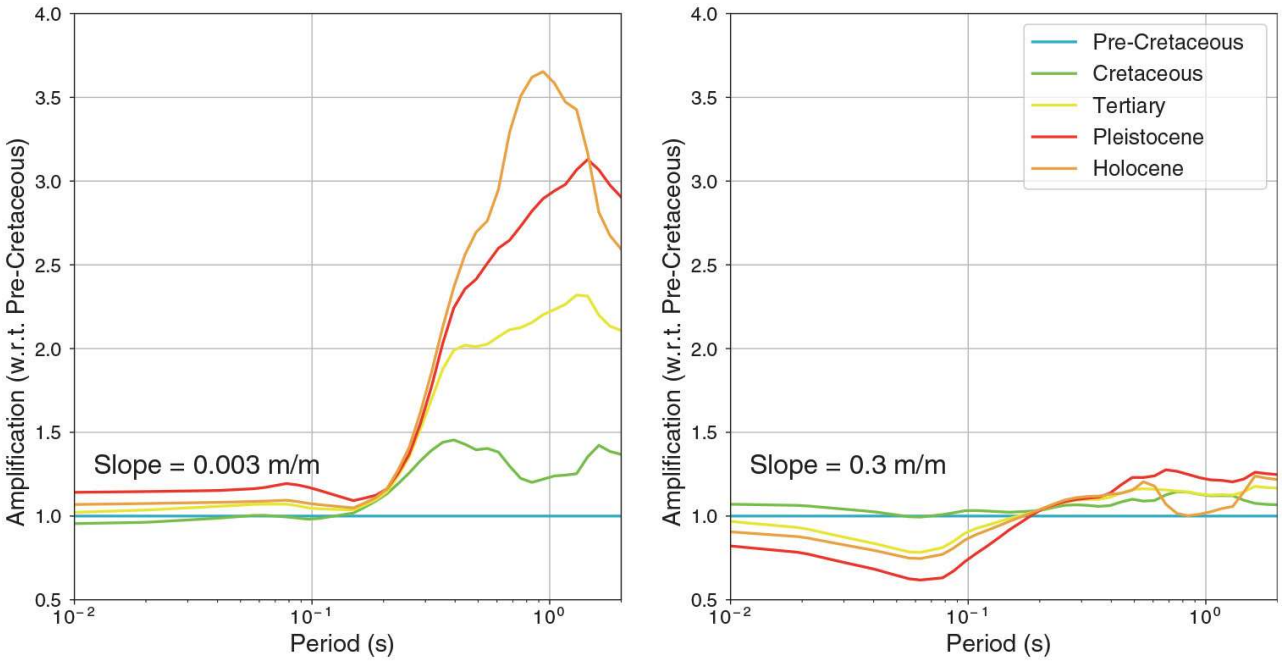

Figure 9. *Spectral variation in amplification with respect to the Pre-Cretaceous condition for a slope of 0.003 m/m (left) and 0.3 m/m (right).*

to the more common application of mixed-effects regression in ground motion modeling to constrain the inter- and intra-event variability, the model in Equation 5 holds both the gradient and intercept (c_{1_g} and c_{2_g}) of the linear model as fixed effects with geology as a random effect, with the correlation in c_{1_g} and c_{2_g} is accounted for explicitly within the model.

Examples of the model fit for Sa(0.2 s) and Sa(1.0 s) are shown in Figures 7 and 8 respectively. In almost all conditions it can be seen that the model fits within the confidence interval of the LOESS regression, with deviation emerging mostly at the extreme lower and higher ranges of the data, which are poorly constrained. As expected, at longer periods, higher c_1 and c_2 replicate the tendency not only toward higher $\delta S2S_S$ in general, but the stronger scaling between slope and amplification, while for the Cretaceous and Pre-Cretaceous periods the virtual absence of correlation between *slope* and $\delta S2S_S$ is preserved, but with systematically negative values that would ensure a clear de-amplification with respect to the center of the data set.

The resulting amplification models for each geological period are shown in Figure 9 for two different slope values, 0.003 m/m and 0.3 m/m. Amplifications are presented with respect to the Pre-Cretaceous category, which for practical purposes here we consider to be representative of a "rock" site. Once again, these factors illustrate how the correlations observed in Figures 7 and 8 translate into practical amplification models. For higher frequency motion, amplification is found only in Holocene and Pleistocene environments on very shallow gradients, while for steeper gradients it is de-amplified with respect to the harder rock conditions. For intermediate to longer period motion at $T > 0.2$, a significantly greater amplification can be seen for almost all geological environments with the highest values around 2.5 to 3.5 on shallow gradients for Quaternary sites.

Using the linear amplification model, with slope mapped at 30 arc-seconds and the digital geological map rasterized at the same resolution, it becomes a straightforward matter to define the site amplification at each grid location in terms of a mean amplification factor and associated variability. An example map of site amplification for Japan inferred from the geologically calibrated slope to

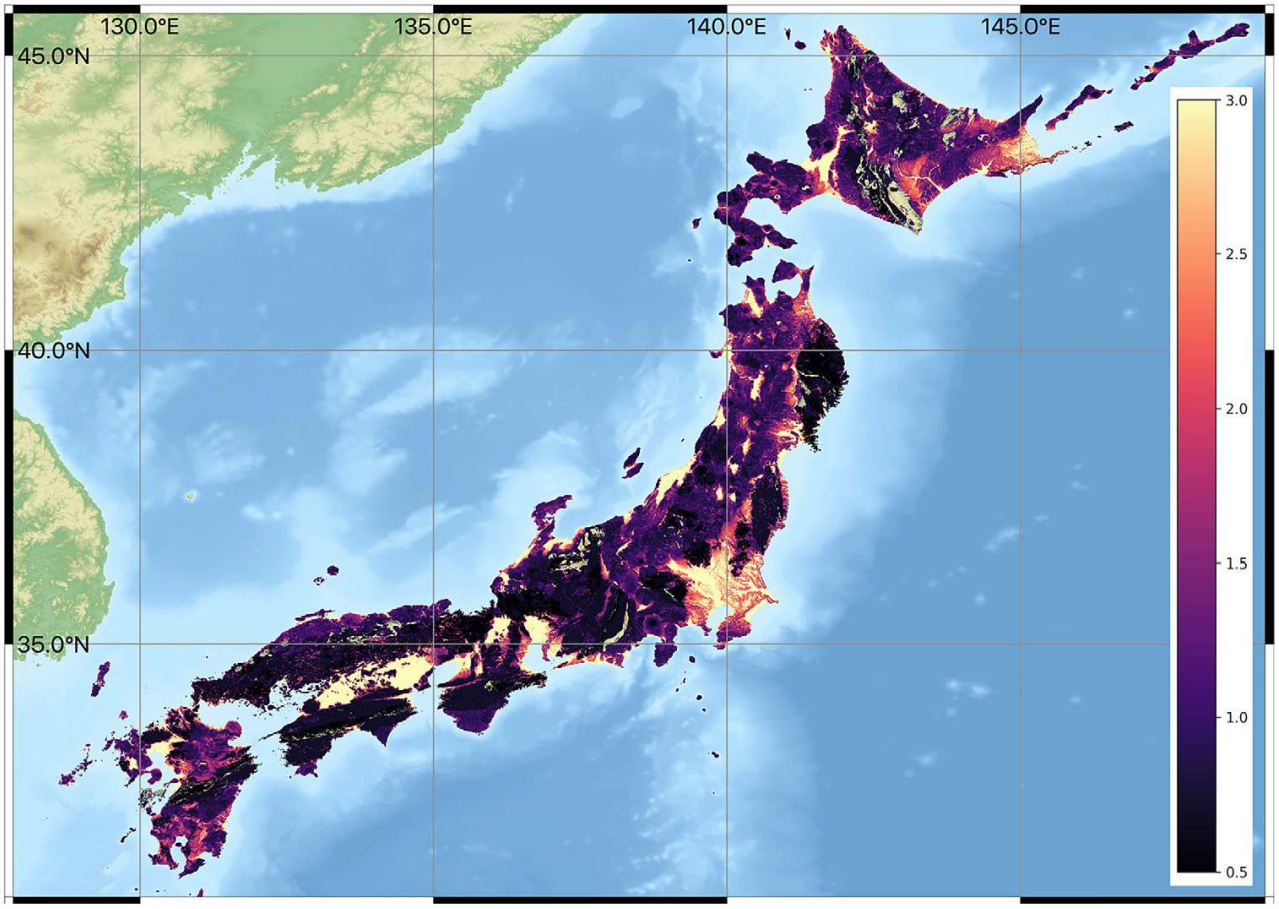

Figure 10. *Implied map of site amplification (with respect to the Pre-Cretaceous condition) for 1.0-s spectral acceleration for Japan based on slope and geology, with the amplification factors indicated in the color scale.*

$\delta S2S_S$ model is shown for SA(1.0s) in Figure 10. While the model shown is by no means a substitute for site-specific investigation, it can be seen clearly that amplification is highest in the lowland and river valleys where low slopes and recent depositional geological units are predominant. Localized amplification in upland valleys can also be seen, implying that the model is capable of resolving some local scale features.

To understand the cost of adopting a model based directly on slope as a site proxy as opposed to the more conventional V_{S3} approach, additional amplification models are developed using the same mixed-effects approach with $\delta S2S_S$ as a function of (1) observed V_{S30} (from the KiK-net station shear-wave velocity profiles) and (2) V_{S30} inferred from Wald and Allen (2007) approach. A two-segment piecewise linear functional form is adopted in the same manner as that of Equation 5, with geological period held as a random effect and a period-independent x_c fixed at $V_{S30} = 1000$ m/s. The fits of the observed V_{S30} model at 0.2 and 1.0-s spectral acceleration are shown in Figures 11 and 12 respectively and show a marked contrast to those of the slope-based model. The stronger correlation between $\delta S2S_S$ and observed V_{S30} is quite evident, and it is expected that a greater degree of amplification can be achieved when observed V_{S30} is adopted. However, a further comparison of the resulting amplification functions from both the observed and inferred V_{S30} forms of the models in Figure 13 highlights some important differences. While the amplification model for observed V_{S30} provides notably higher amplification factors for shorter periods, the amplification factors implied by the inferred V_{S30} model are comparable to those from the slope model, with the differences between the two diminishing (though not disappearing) at longer spectral periods. This demonstrates that the

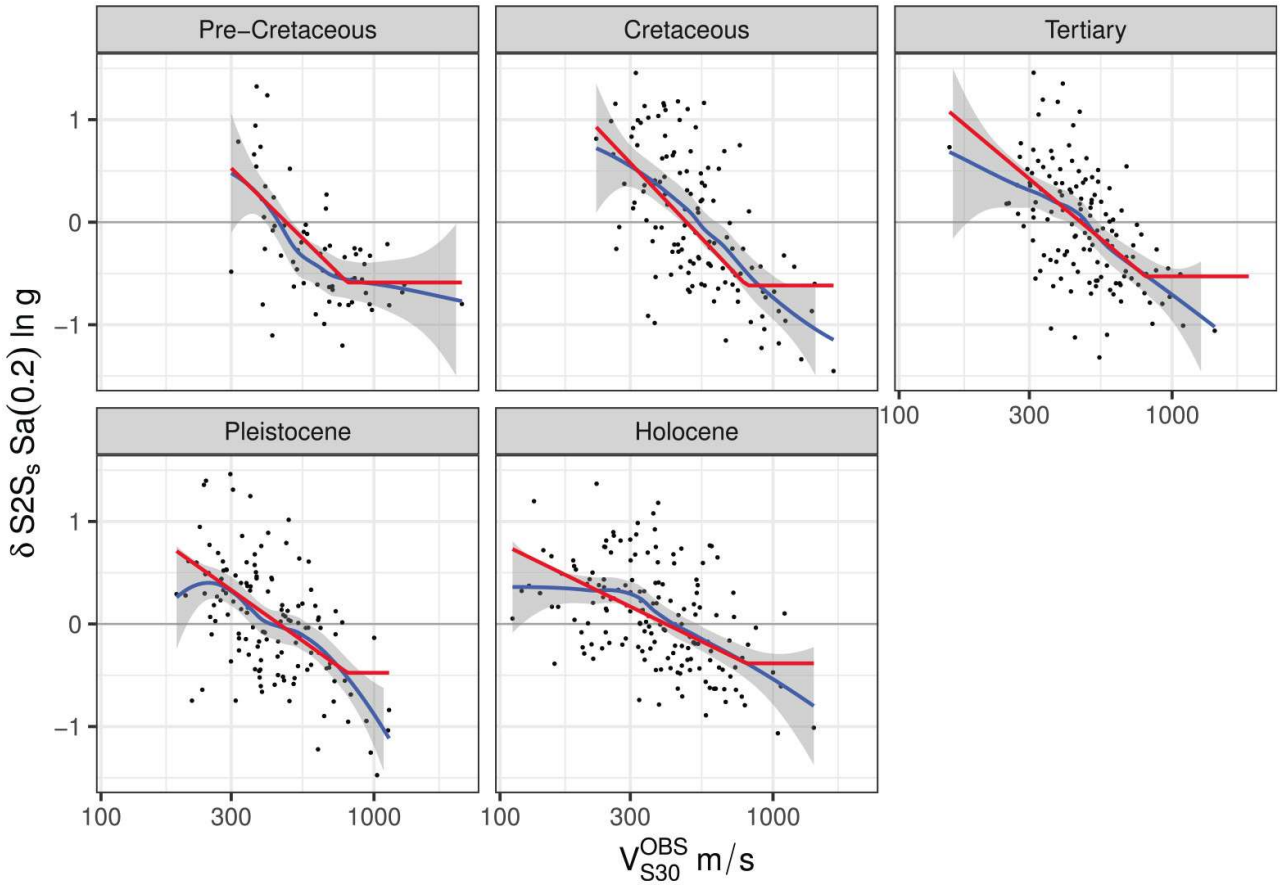

Figure 11. *Fit of mixed-effect amplification model based on observed V_{S30} for each of the considered geological units for Sa(0.2 s).*

use of inferred V_{S30} as a site proxy would not necessarily capture the degree of amplification in ground motion implied from the correlation with observed V_{S30}, yet it seems to offer a similar degree of amplification to that of using slope alone.

A critical comparison of the methods should also consider the resulting variability, σ_s, and in Figure 14 this term is compared for the three predictor variables (*slope*, observed V_{S30}, and inferred V_{S30}), both for the case in which geology is included as a random effect and when it is excluded. First, a moderate reduction in σ_s is achieved with the inclusion of geology, the degree of which becomes longer with spectral period. This is advantageous as in the current case mapped geology is known for each site and can therefore reduce uncertainty at minimal cost. As expected, variability is notably smaller when observed V_{S30} is used as the predictive parameter. However, when inferred V_{S3} values are used there is little distinct reduction in variability compared to using slope alone once geology is included. There are several implications to this, this first being that inferred and observed site properties produce neither the same degree of amplification nor a comparable variability in amplification, meaning that they should not be used interchangeably, or else the coefficients of the model should be different for the two cases (e.g., Abrahamson et al., 2014). The second implication is that once geology is accounted for in the slope model there is virtually no discernable reduction in uncertainty using a topographically inferred proxy as a predictor variable rather than just using the topography directly. This latter point is compounded by the fact that the inferred proxy is itself uncertain with respect to the topography and its correlation with the site property (in this case V_{S30}) highly dependent on the geological conditions. By contrast, the topographic properties are known or can be derived directly from DEM data to within a small degree of measurement error, and their relation to

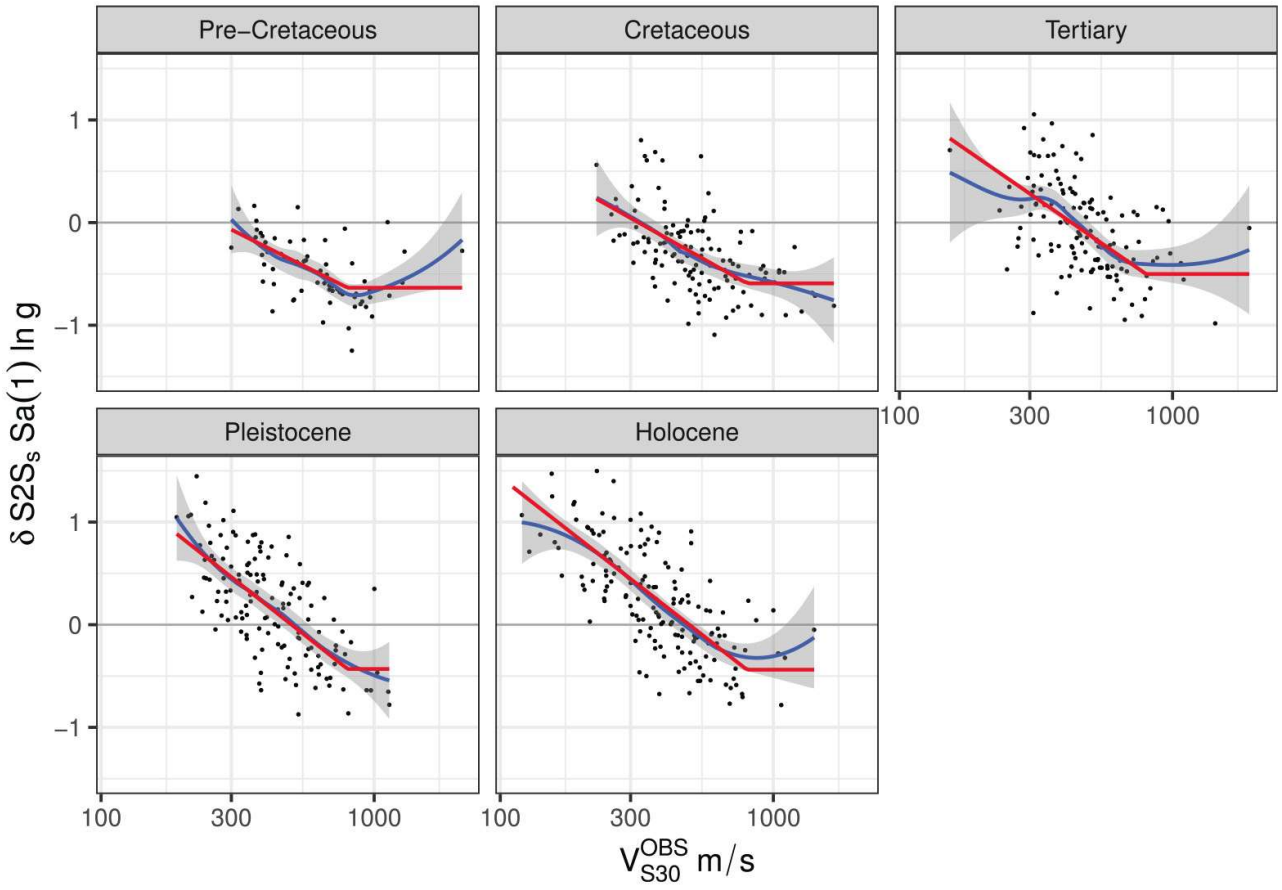

Figure 12. *As Figure 11 for Sa(1.0 s).*

amplification calibrated according to the geological conditions themselves even if this means they may be extremely weak predictors of amplification in some environments.

Also shown in Figure 14 is the comparison of the total standard deviation σ_T that would result from combining the various observed/inferred V_{S30} and/or slope models with the inter-event variability, τ, to get the total aleatory variability of the Kotha et al. (2018) ground motion model. Additional total variabilities are shown as a point of comparison with the total ergodic sigma of the model presented here. These include both the site-to-site variability ϕ_{S2S} and the single-station variability ϕ_0 such that $\sigma_T = \sqrt{\tau^2 + \phi_{S2S}^2 + \phi_0^2}$, as well as the partially ergodic single-station sigma of the model when $\delta S2S_S$ is known ($\sigma_T = \sqrt{\tau^2 + \phi_0^2}$). These two uncertainties reflect, respectively, the case when

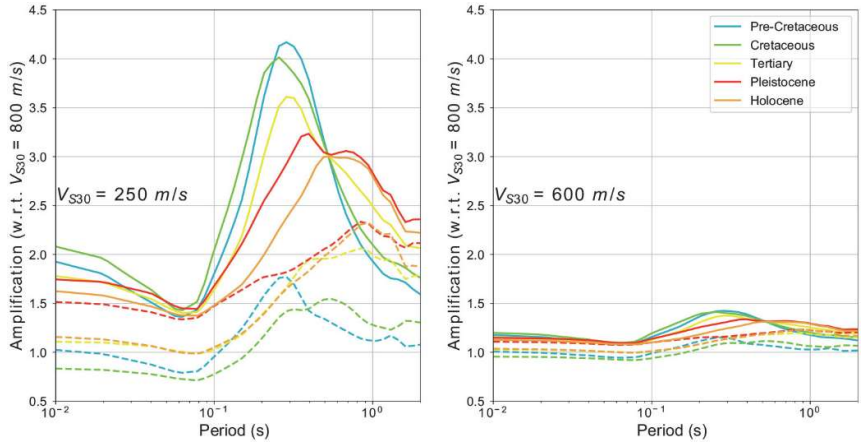

Figure 13. *Comparison of amplification on soft soil V_{S3} = 200 m/s and stiff soil V_{S3} = 600 m/s, with respect to V_{S30} = 800 m=s, predicted by geologically calibrated V_{S30} models for (i) observed V_{S30} (continuous lines) and (ii) inferred V_{S3} from topography (dashed lines).*

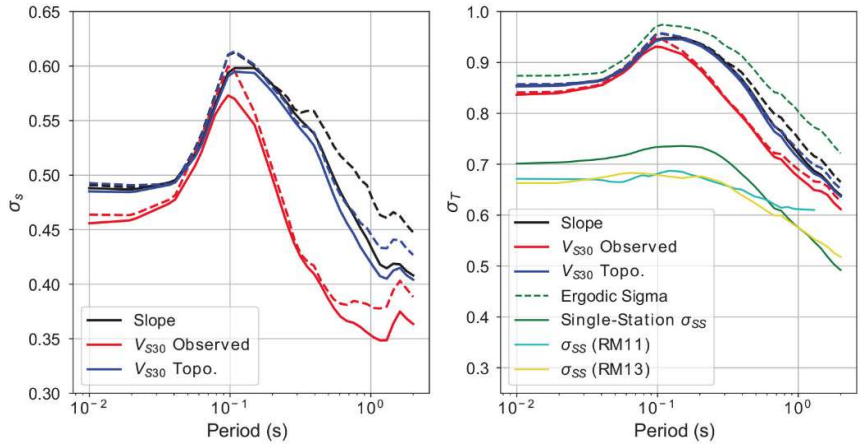

Figure 14. *Variation with spectral period of the standard deviations of site amplification model, σ_S of Equation 5 (left) and the resulting total variability of the ground motion model σ_T (right), with respect to slope, observed V_{S30}, and inferred V_{S3} , ε_S excluding dependence on geological period (dashed line) and including geological period (solid line). Fully ergodic σ_T and single-station σ_T from Kotha et al. (2018) are shown in the dashed and solid green lines respectively. Additional single-station sigma models from Rodriguez-Marek et al. (2011) (RM11) and Rodriguez-Marek et al. (2013) (RM13) are shown in cyan and yellow respectively.*

no site information is known and when the site-specific amplification $\delta S2S_S$ is known exactly, and as such envelope the range of uncertainties from the other predictors. The single-station sigma (σ_{SS}) is also compared against that of Rodriguez-Marek et al. (2011) and Rodriguez-Marek et al. (2013), the former derived from surface records in the KiK-net data set and the latter from an exploration of σ_{SS} across the globe. It can be seen that σ_{SS} in the new model is higher at shorter periods, and lower at longer periods, than those of previous studies, which we attribute to an increase in ϕ_0 in the new data set for higher frequency motion. Collectively, these models demonstrate the capacity for reduction in uncertainty if $\delta S2S_S$ is known for the site, which can only be achieved through repeated observations of ground motion for that given site.

Depth to bedrock

While the relatively simple linear model in Equation 5 can be shown to predict amplification, an important question to ask is to what extent this can capture the influence of deeper basin effects? From the KiK-net site profiles, the depth to the 1000-m/s shear-wave velocity horizon (Z_{1000}) is determined as a common proxy for basin depth. Using the residuals of the model shown in Equation 5, ε_S, at Sa(1.0 s), Figure 15 demonstrates that there still exists a clear trend in the residuals with basin depth, and that this is present across most geological environments.

The identification of potential proxies from which basin amplification could be inferred on a regional scale remains elusive. Figure 16 displays the general trends in the residual ε_S of the slope-based amplification model using the Pelletier et al. (2016) sedimentary basin thickness data set, but demonstrates that there is no coherent trend of the sort seen in Figure 15. Although there does exist for Japan a reference shallow velocity model, which would in the current case permit the resolution of basin depth variation at the spatial scale required here, few such velocity models currently exist on a national or regional scale that would permit transferability to other regions of the globe. The same residual trends have been explored for other proxies that have a theoretical connection to sedimentary basin thickness, such as elevation or gravity anomaly, but no statistically significant trends have yet been identified.

While the search for explicit mappable proxies for basin thickness has yet to identify potential candidates, it is important to note that the influence of deeper basin effects is not necessarily absent

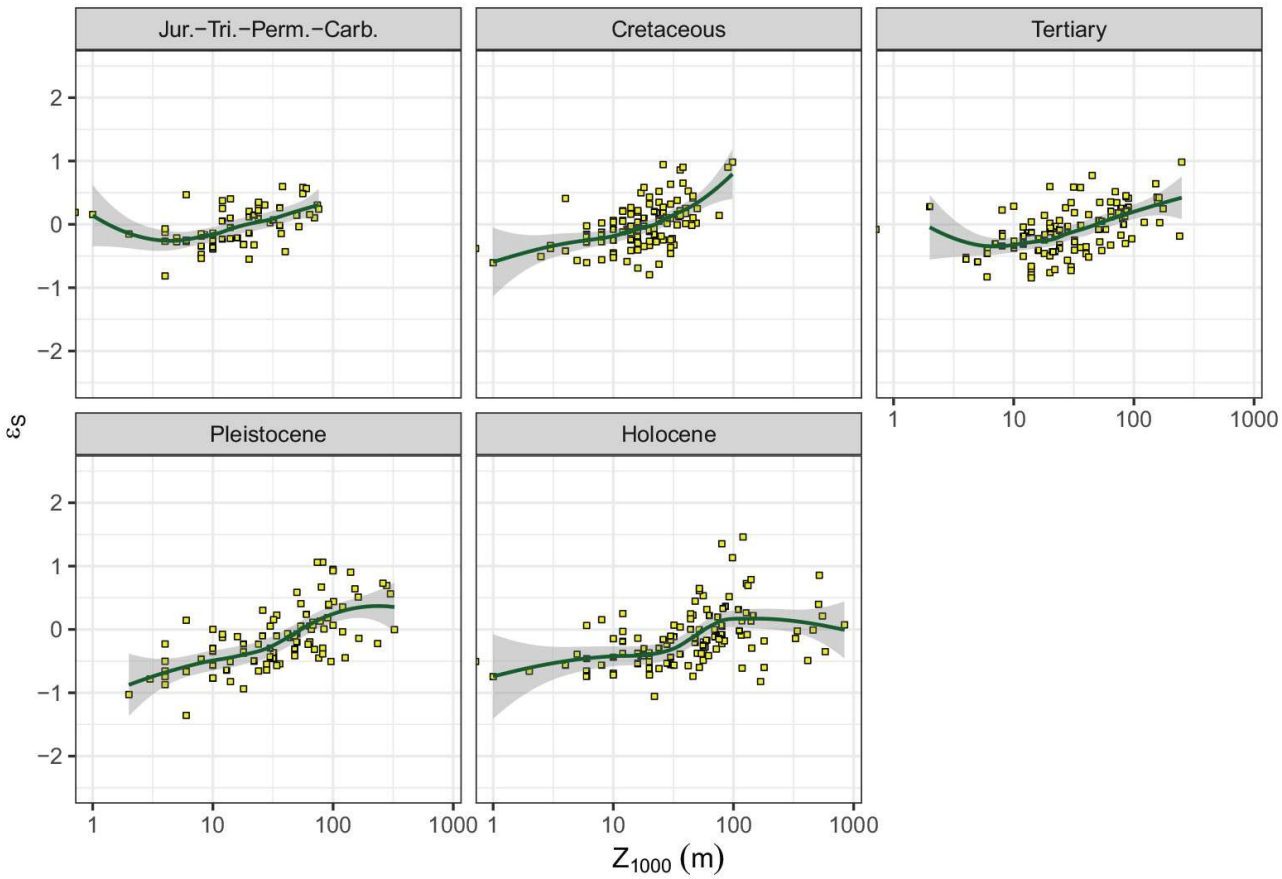

Figure 15. *Correlation between the residual values with respect to Equation 5 and depth to the 1000-m/s shear-wave velocity horizon for the KiK-net sites.*

from the correlations shown in Figure 8, as basin depth cannot be considered entirely independent of topographic slope in some environments. Indeed, for Holocene deposits, where one might expect the greatest sedimentary thickness, correlation between slope and basin depth is evident particularly for sites with basin depths greater than 50 m (Figure 17). Therefore, one cannot consider slope to be a uniquely shallow parameter from which to constrain site amplification. Although we note that the nonparametric LOESS regression indicates the amplification model may be less biased with respect to Z_{1000} on those same thick Holocene sites where the correlation with slope is strongest, supporting the notion that, partially at least, some basin amplification is entrained into the slope and geology-based model.

Discussion

Considerations for application

The feasibility of using regional geology as a means of calibrating amplification models that depend on mappable proxies is demonstrated here, but for broader application there are additional implications in this process as to how one should then approach ground motion modeling on a regional scale. The site-to-site residuals ($\delta S2S_S$) are not only dependent on the GMM itself, they would ideally require multiple recordings at a sufficient number of stations in order to be determined with a higher degree of statistical confidence. Inevitably, a minor proportion of the larger variability associated with the slope and geology-based amplification model results from epistemic uncertainty in the site-to-site residuals of the stations themselves. Furthermore, in low-seismicity regions a significant

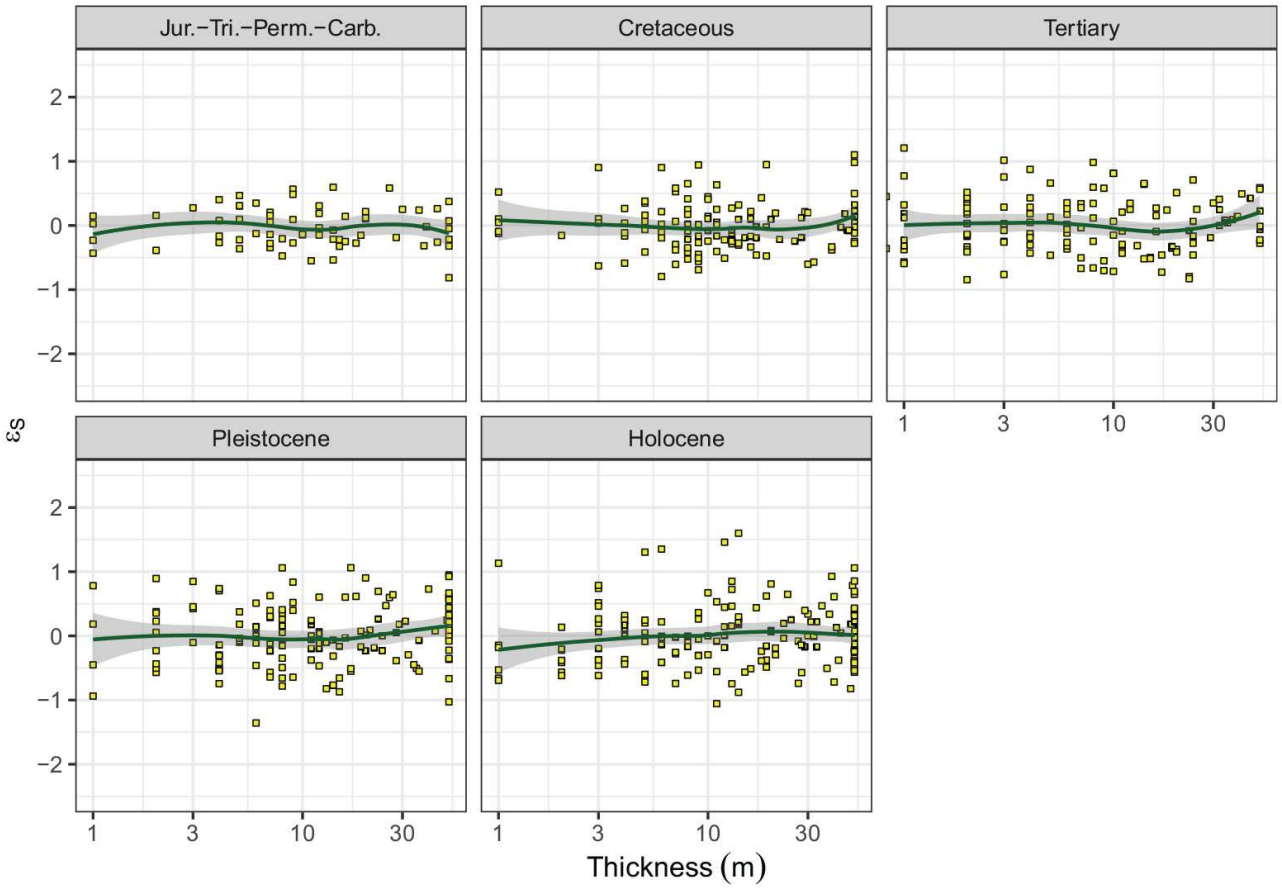

Figure 16. *Correlation between the residual values for the model at Sa(1.0 s) with respect to Equation 5 and the inferred sediment thickness model of Pelletier et al. (2016).*

amount of time may be required before sufficient strong motion recordings could be obtained, although the feasibility of inferring amplification factors from weak motion data should be explored.

In light of the importance of observed strong motion data, an obvious question to ask is how such an approach could be applied in regions where data is limited, and what, if anything, could be undertaken in areas where no strong motion data are available? This adds further weight to the established consensus that more instrumentation and improved acquisition of metadata are fundamental to the development GMMs for seismic risk analysis and mitigation purposes in the future. Likewise, there emerges a new requirement, which is that the availability of, and ongoing refinements to, high-resolution digital geological maps for a region may now have a demonstrable impact in the improvement of earthquake risk assessments. In the shorter term, an expansion of this approach to other well-recorded regions is desirable.

The dependence of this approach on the GMM may make the common practice of constructing logic trees from multiple GMMs difficult to sustain. Instead by connecting the amplification model directly to the site-to-site residuals of a well-calibrated GMM (or GMMs) for a region, there is a stronger case for the adoption of "backbone" approach to characterization of ground motion epistemic uncertainty (Atkinson et al., 2014). This builds the ground motion logic tree around a single model (or smaller number of well-calibrated models), applying scaling factors for source and path properties to account for limitations in the knowledge of ground motions in the region.

While the methods described above demonstrate that a regional amplification model can be developed using amplifications at strong motion recording stations combined with and mappable

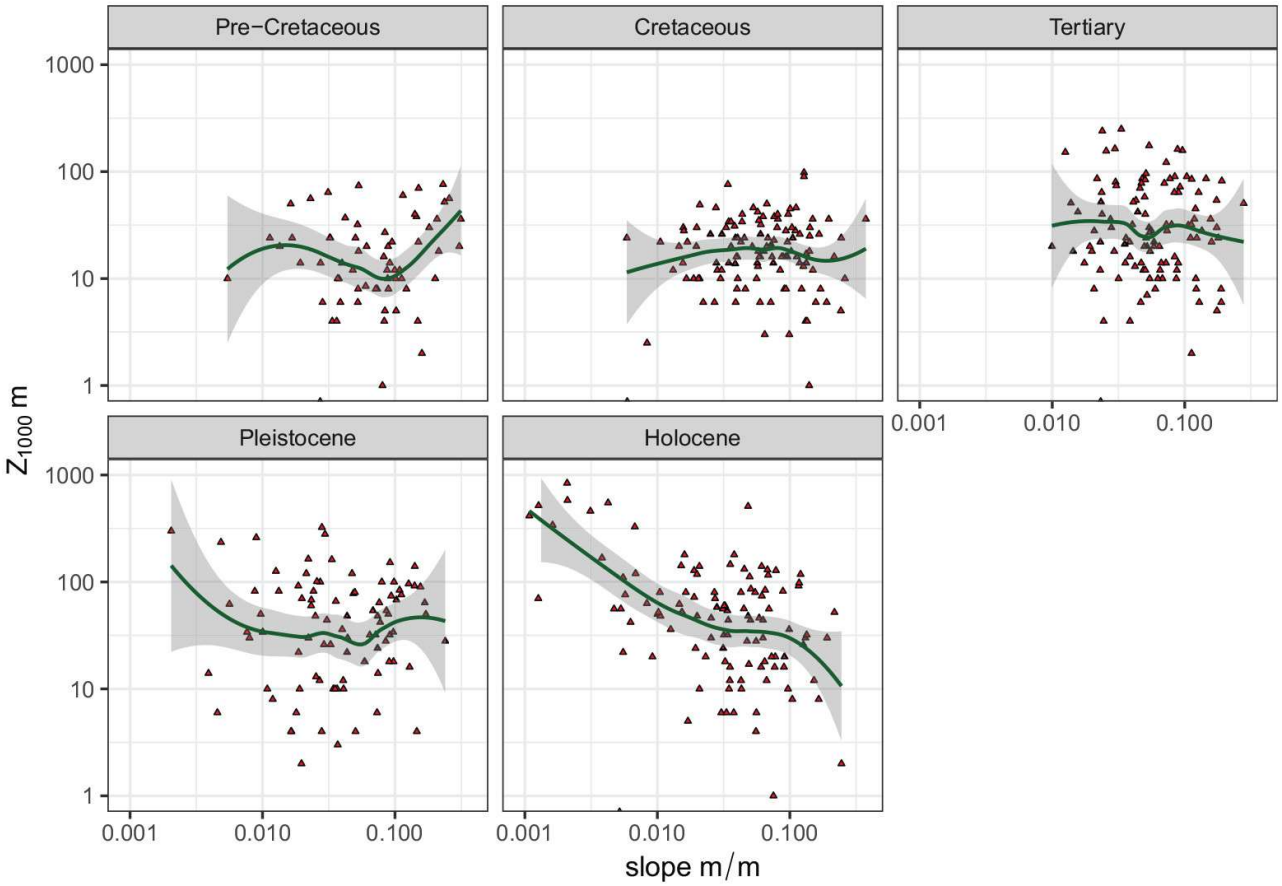

Figure 17. *Trends between slope and depth to the 1000-m/s shear-wave velocity horizon sorted by geological period.*

proxies, it is important to take note of some of the caveats inherent within this process. The first is dependence upon the quality of the digital geological data set in terms of both its spatial resolution and its lithological classifications. In the case of Japan, the digital geological map is of a particularly high resolution that it is able to identify the boundaries of different geological environments with a reasonable accuracy and hence, that the assignment of KiK-net stations to their respective geological units is done with some confidence. Likewise, this also assumed that accuracy in the location of the strong motion stations is itself comparable, and it can be easily demonstrated that rounding of the station's longitudes and latitudes to the nearest two or three decimal places increases the potential for misclassification. Indeed, several stations that were initially unassigned to geological units were subsequently inspected and in the majority of cases the reported locations from KiK-net would place them between 20 and 50-m offshore or into a water body, thus laying outside of the geological map. Naturally, there is the possibility that some KiK-net locations have been mis-assigned to the geology and that this may be contributing toward the uncertainty. Potentially, this could be refined by focusing on outliers in the models or even inspecting carefully stations lying close to the boundaries of their respective geological units.

The second obvious limitation in this process is the difficulty to capture nonlinearity in amplification within the model. Further efforts currently being directed at attempting to fit such a model, yet the significant uncertainty in the use of slope and/or proxy V_{S30}, even when calibrated to a particular geological period, would make nonlinearity difficult to constrain in a model derived only from observations of $\delta S2S_S$. Work is ongoing to explore this particular problem, though it is worth re-iterating the objectives stated earlier in the article that the use of slope and geology is intended as a practical

means of implementing site amplification in a regional scale risk assessment, and that it is not presented as the optimum proxy (nor as the optimum amplification model) in site-specific locations where detailed site information can be obtained. As such, attempting to introduce nonlinearity into the amplification may give a false confidence as to what can be achieved from models based on proxies of this nature. That being said, the geological environment is critical in determining conditions where nonlinearity may be expected in soil amplification, suggesting that the methods presented here may come to assume greater significance in the role of nonlinear amplification modeling as more strong motion observations emerge.

In addition to the potential limitations relating to data quality and the ability to capture certain aspects of the site amplification, there is an obvious question of the transferability of this approach to other regions. It would be relatively straightforward task to replicate analyses such as these in regions where sufficient strong motion data exist (e.g., Western US, Southern Europe, New Zealand, Taiwan). More questionable, however, would be to apply the amplification factors derived in this data set to regions with a substantially different lithological composition and/or geological history. For example, the chronology of glaciations in a region will likely influence the nature of the velocity profiles with respect to the given geological environment, such as the presence of shallow soils overlaying hard rock with a strong impedance contrast (as is commonly observed in Japan) versus environments of similar geological age in which the site profiles are more gradational (as is more common in California). In such a case one might expect a tendency in Japan toward higher amplifications across a range of periods than in the gradational environments. To what extent this variability in profile explains much of the uncertainty in the amplification functions is unclear, but users must be aware of this should they attempt to transfer amplification function from one region to another. A better approach in the long term would be to consolidate strong motion data, station information, and geology on a global scale and explore regional differences in amplification per geological period as a further nested random effect, resulting in a geological period–specific amplification function that can be calibrated to different environments when data permit, and still applied in their general form elsewhere.

In spite of these limitations, however, it is important to emphasize that the approach for regional modeling being presented here might should be considered as a baseline that would provide amplification factors, and corresponding uncertainties, that could be applied at a regional scale. Such an approach, however, does not exclude the possibility that where detailed site information can be retrieved and amplification functions, and their respective uncertainties, calibrated at a site- or city-specific scale from microzonation studies there is ample scope to adopt these calibrated factors where appropriate.

Conclusion

The exploration of site-to-site ground motion residuals from the Japanese KiK-net data, and in particular the correlations with slope and geology, has led to a potential pathway for modeling site amplification in seismic risk at regional scales. This approach diverges from the more widely adopted application of V_{S30} derived from topographic data, as it seeks to connect the amplification directly to the mappable proxies with the increased uncertainty explicitly accounted for in the amplification model. It is demonstrated here that as a predictor of local site response, topographically inferred V_{S30} seems to provide little improvement over direct use of topographic data in terms of capturing both the degree of amplification or the reduction of uncertainty. Furthermore, the correlation between *slope* and V_{S3} appears highly dependent on the geological environment itself, as has been

demonstrated in previous studies (e.g., Kwok et al., 2018; Thompson et al., 2014; Vilanova et al., 2018). As a result, simple application of topographically inferred V_{S30} without appropriate adjustments may produce potentially erroneous amplifications, for example, predicting higher ground motions on flat terrain even in regions of older and harder surface rocks. That being said, however, the inclusion of geology as a random effect in the amplification model did produce a reduction in aleatory uncertainty when using either topographic slope directly or the topographically inferred V_{S30}, which would suggest that incorporation of geology could be used to enhance the capability of inferred V_{S30} to predict site amplification if one does not wish to abandon its usage altogether.

While this approach cannot be considered a substitute for detailed site-specific investigation or microzonation, by relating the amplification directly to the mappable parameters the resulting uncertainties can be integrated into the seismic risk calculation more explicitly inside the aleatory variability of the GMM. The penalty in terms of a higher σ is both appropriate given the lack of information on these scales and practical in terms of requiring the risk modeler to use data that are available over the region of interest. This approach also has the flexibility to be adapted to various exposure resolutions, with the mean amplification and its associated variability possible to calibrate to the potentially coarser resolution of the exposure model. Further efforts are needed to explore the transferability of this approach to different regions, with a model for Europe now in development, and to identify other potential mappable proxies that could help to refine and improve predictions. Tentative applications using European strong motion data also reveal similar trends in terms of the correlation between *slope* and $\delta S2S_S$ for those geological periods common to both the European and Japanese geological data. This may suggest a degree of transferability of models from one region to another, though further analysis of strong motion data sets from other regions of the globe is ongoing to determine if this could be a suitable strategy. In the longer term, this approach also provides a clear and direct framework through which dense seismic monitoring and the acquisition and dissemination of geological and geomorphological data can improve the practice of seismic risk mitigation in the future.

Acknowledgements

The authors are sincerely grateful to both the National Research Institute for Earth Science and Disaster Resilience (NIED) for their ongoing curation of the KiK-net strong motion database and the Geological Survey of Japan for access to the high-resolution Seamless Digital Geological Map of Japan. Finally, we wish to thank Marco Pagani, Trevor Allen, and two anonymous reviewers, whose insightful comments helped improve this manuscript.

Authors' Note

Sreeram Reddy Kotha is now affiliated with Grenoble Alpes University, Savoie Mont Blanc University, CNRS, IRD, IFSTTAR, ISTerre, Grenoble, France.

Declaration of conflicting interests

The author(s) declared no potential conflicts of interest with respect to the research, authorship, and/or publication of this article.

Funding

The author(s) disclosed receipt of the following financial support for the research, authorship, and/or publication of this article: This investigation has been funded, in part, by the Horizon 2020 "Seismology and Earthquake Engineering Research Infrastructure Alliance for Europe (SERA)" project and the contributions of Sreeram Reddy Kotha (second author) in this research are funded by the SIGMA2 consortium (EDF, CEA, PG&E, SwissNuclear, Areva, CEZ, CRIEPI) under grant– 2017–2021.

ORCID iD
Graeme Weatherill https://orcid.org/0000-0001-9347-2282

References

Abrahamson AA, Silva WJ and Kamai R (2014) Summary of the ASK14 ground motion relation for active crustal regions. Earthquake Spectra 30: 1025–1055.

Al Atik L, Abrahamson N, Bommer JJ, et al. (2010) The variability of ground-motion prediction models and its components. Seismological Research Letters 81: 794–801.

Allen TI and Wald DJ (2009) On the use of high-resolution topographic data as a proxy for seismic site conditions (V_{s30}). Bulletin of the Seismological Society of America 99: 935–943.

Atkinson GA, Bommer JJ and Abrahamson NA (2014) Alternative approaches to modeling epistemic uncertainty in ground motions in probabilistic seismic-hazard analysis. Seismological Research Letters 85: 1141–1144.

Bates D, Mächler M, Bolker BM, et al. (2015) Fitting linear mixed-effects models using lme4. Journal of Statistical Software 67: 1–48. doi:10.18637/jss.v067.i01

Chiou BS-J and Youngs RR (2014) Update of the Chiou and Youngs NGA Model for the average horizontal component of peak ground motion and response spectra. Earthquake Spectra 30: 1117–1153.

Dawood HM, Rodriguez-Marek A, Bayless J, et al. (2016) A flatfile for the KiK-net database processed using and automated protocol. Earthquake Spectra 32: 1281–1302.

Derras B, Bard PY and Cotton F (2017) Vs30, slope, H800 and f0: Performance of various site condition proxies in reducing ground-motion aleatory variability and predicting nonlinear site response. Earth, Planets and Space 69: 1–21.

Geological Survey of Japan (2014) Seamless digital geological map of Japan (1:200,000). Tech report, January. Tokyo, Japan: Geological Survey of Japan.

Kotha SR, Cotton F and Bindi D (2018) A new approach to site classification: Mixed-effects ground motion prediction equation with spectral clustering of site amplification functions. Soil Dynamics and Earthquake Engineering 110: 318–329.

Ktenidou OJ, Roumelioti Z, Abrahamson N, et al. (2018) Understanding single-station ground motion variability and uncertainty (sigma): Lessons learnt from EUROSEISTEST. Bulletin of Earthquake Engineering 16: 2311–2336.

Kwok OLA, Stewart JP, Kwak DY, et al. (2018) Taiwan-specific model for V_{s30} prediction considering between-proxy correlations. Earthquake Spectra 34: 1973–1993.

Lemoine A, Douglas J and Cotton F (2012) Testing the applicability of correlations between topographic slope and V_{s30} for Europe. Bulletin of the Seismological Society of America 102: 2585–2599.

Okada Y, Hori S, Obara K, et al. (2004) Recent progress of seismic observation networks in Japan—Hi-net, F-net, K-NET and KiK-net. Earth Planets Space 56: xv–xxviii.

Pagani M, Monelli D, Weatherill G, et al. (2014) OpenQuake Engine: An open hazard (and risk) software for the global earthquake model. Seismological Research Letters 85: 692–702.

Pelletier JD, Broxton PD, Hazenberg P, et al. (2016) A gridded global data set of soil, intact regolith, and sedimentary deposit thicknesses for regional and global land surface modeling. Journal of Advances in Modeling Earth Systems 8: 41–65.

Rodriguez-Marek A, Cotton F, Abrahamson NA, et al. (2013) A model for single-station standard deviation using data from various tectonic regions. Bulletin of the Seismological Society of America 103: 3149–3163.

Rodriguez-Marek A, Montalva G, Cotton F, et al. (2011) Analysis of single-station standard deviation using the KiK-net data. Bulletin of the Seismological Society of America 101: 1242–1258.

Stewart JP, Afshari K and Goulet CA (2017) Non-ergodic site response in seismic hazard analysis. Earthquake Spectra 33: 1385–1414.

Thompson EM and Wald DJ (2012) Developing Vs30 site-condition maps by combining observations with geologic and topographic constraints. In: Proceedings of the 15th world conference on earthquake engineering, Lisbon, 24–28 September.

Thompson EM, Wald DJ and Worden CB (2014) A V_{s30} map for California with geological and topographic constraints. Bulletin of the Seismological Society of America 104: 2313–2321.

Vilanova SP, Narciso J, Carvalho JP, et al. (2018) Developing a geologically based V_{s30} site-condition model for Portugal: Methodology and assessment of the performance of proxies. Bulletin of the Seismological Society of America 108: 322–337.

Wald DJ and Allen TI (2007) Topographic slope as a proxy for seismic site conditions and amplification. Bulletin of the Seismological Society of America 97: 1379–1395.